

## CORRECTION

# Impulsive ankle push-off powers leg swing in human walking

Susanne Lipfert, Michael Günther, Daniel Renjewski and Andre Seyfarth

There was an error in *J. Exp. Biol.* **217**, 1218-1228. A reference was missing from the reference list. The reference is listed below.

Zelik, K. E., Huang, T. W., Adamczyk, P. G. and Kuo, A. D. (2014). The role of series ankle elasticity in bipedal walking. *J. Theor. Biol.* **346**, 75-85.

We apologise to the authors and readers for this omission.

## RESEARCH ARTICLE

# Impulsive ankle push-off powers leg swing in human walking

 Susanne W. Lipfert<sup>1,\*</sup>, Michael Günther<sup>2,3</sup>, Daniel Renjewski<sup>4</sup> and Andre Seyfarth<sup>5</sup>

## ABSTRACT

Rapid unloading and a peak in power output of the ankle joint have been widely observed during push-off in human walking. Model-based studies hypothesize that this push-off causes redirection of the body center of mass just before touch-down of the leading leg. Other research suggests that work done by the ankle extensors provides kinetic energy for the initiation of swing. Also, muscle work is suggested to power a catapult-like action in late stance of human walking. However, there is a lack of knowledge about the biomechanical process leading to this widely observed high power output of the ankle extensors. In our study, we use kinematic and dynamic data of human walking collected at speeds between 0.5 and 2.5 m s<sup>-1</sup> for a comprehensive analysis of push-off mechanics. We identify two distinct phases, which divide the push-off: first, starting with positive ankle power output, an alleviation phase, where the trailing leg is alleviated from supporting the body mass, and second, a launching phase, where stored energy in the ankle joint is released. Our results show a release of just a small part of the energy stored in the ankle joint during the alleviation phase. A larger impulse for the trailing leg than for the remaining body is observed during the launching phase. Here, the buckling knee joint inhibits transfer of power from the ankle to the remaining body. It appears that swing initiation profits from an impulsive ankle push-off resulting from a catapult without escapement.

**KEY WORDS:** Push-off, Power amplification, Catapult, Joint force power, Impulse, Jerk

## INTRODUCTION

Steady-speed walking over level ground is a cyclic motion where the average mechanical energy of the body is constant over time. But of course, force must be produced to support the body weight and work must be done to lift and propel the body. These demands may be met most economically by muscles that produce force while minimizing mechanical work. Muscle–tendon units can operate like springs, storing and recovering mechanical energy as the limbs flex and extend (Cavagna et al., 1964; Alexander and Bennet-Clark, 1977; Heglund et al., 1982; Hof, 1998; Blickhan, 1989; McMahon and Cheng, 1990). Most of this spring-like function can be performed passively by the stretch and recoil of leg tendons, while muscle fibers actively maintain tension on the spring, developing force with little or no shortening velocity (Roberts et al., 1997; Lichtwark and Wilson, 2006).

<sup>1</sup>Human Motion Engineering, 5021 SW Philomath Boulevard, Corvallis, OR 97333, USA. <sup>2</sup>Institut für Sport- und Bewegungswissenschaft, Universität Stuttgart, Allmandring 28, D-70569 Stuttgart, Germany. <sup>3</sup>Institut für Sportwissenschaft, Friedrich-Schiller-Universität, Seidelstraße 20, D-07749 Jena, Germany. <sup>4</sup>Dynamic Robotics Laboratory, Oregon State University, 021 Covell Hall, Corvallis, OR 97333, USA. <sup>5</sup>Institut für Sportwissenschaft, Technische Universität Darmstadt, Magdalenenstrasse 27, D-64289 Darmstadt, Germany.

\*Author for correspondence (lipfert@human-motion-engineering.org)

Received 18 September 2013; Accepted 19 November 2013

It has been demonstrated in the literature (Fukunaga et al., 2001; Ishikawa et al., 2005; Lichtwark et al., 2007; Cronin et al., 2013) that the tendons of the human ankle extensors stretch slowly during the single support phase of walking and then recoil rapidly during late stance, while the fibers operate near-isometrically. This interaction between muscle fibers and the attached tendon allows the overall muscle–tendon unit to operate with high power output and efficiency. Power-amplifying mechanisms have been depicted as catapults, where relatively slow muscle contractions precede rapid movement (Bennet-Clark, 1975; Alexander, 1988). As muscles provide the necessary force, elastic potential energy is stored in elastic elements while a catch of some sort (e.g. a latch or antagonistic muscle activity) prevents the movement until a later time (Gronenberg, 1996; Nishikawa, 1999; Burrows, 2003; Wilson et al., 2003; Patek et al., 2007). In human walking, such function allows higher ankle power output than what muscle fibers could produce (for power output of muscle fibers of the ankle extensors, see Appendix 1). However, a mechanical description of how this actually happens is missing.

High power action of the ankle extensors during late stance in human walking has been described in a large number of studies (e.g. Hof et al., 1983; Ishikawa et al., 2005; Donelan et al., 2002b; Sawicki et al., 2009). But there is controversy about the biomechanical function of the ankle extensors, as research by Meinders et al. (Meinders et al., 1998) shows. On the one hand, it has been argued that mechanical energy is dissipated at the beginning of each step, as negative work is performed on the center of mass (CoM) in a mechanical collision between the leading leg and the ground. To power level walking, positive work done by the trailing leg has been discussed as one method of actuation to restore the lost energy by impulsively pushing off the ground before heel strike of the leading leg (McGeer, 1990; Donelan et al., 2002a; Donelan et al., 2002b; Kuo, 2002; Collins et al., 2005; Dean and Kuo, 2009). On the other hand, other research implies that only a small part of the energy generated during push-off is propagated through the knee joint and even less through the hip (Winter and Robertson, 1978; Hof et al., 1992). Therefore, work done by the ankle extensors was suggested to provide kinetic energy for initiation of the swing phase (Bajd et al., 1997; Meinders et al., 1998).

In our study, we aim to describe the mechanism behind the remarkable power peak observed during ankle push-off in human walking. We propose a catapult without escapement, where elastic energy stored in the ankle extensors is released by alleviating body mass from the trailing leg. The much smaller mass of the trailing leg is then accelerated into swing. We support our suggestion by calculating the linear power transfer between the trailing leg and the upper body as well as their impulses throughout two phases of the push-off. These are, first, an alleviation phase, where the trailing leg is alleviated from supporting the body mass, and second, a launching phase, where stored energy in the ankle joint is released.

## RESULTS

Fig. 1 shows the dynamics of the lower limb and the ground reaction force (GRF) vector for the stance phase of walking. An extending

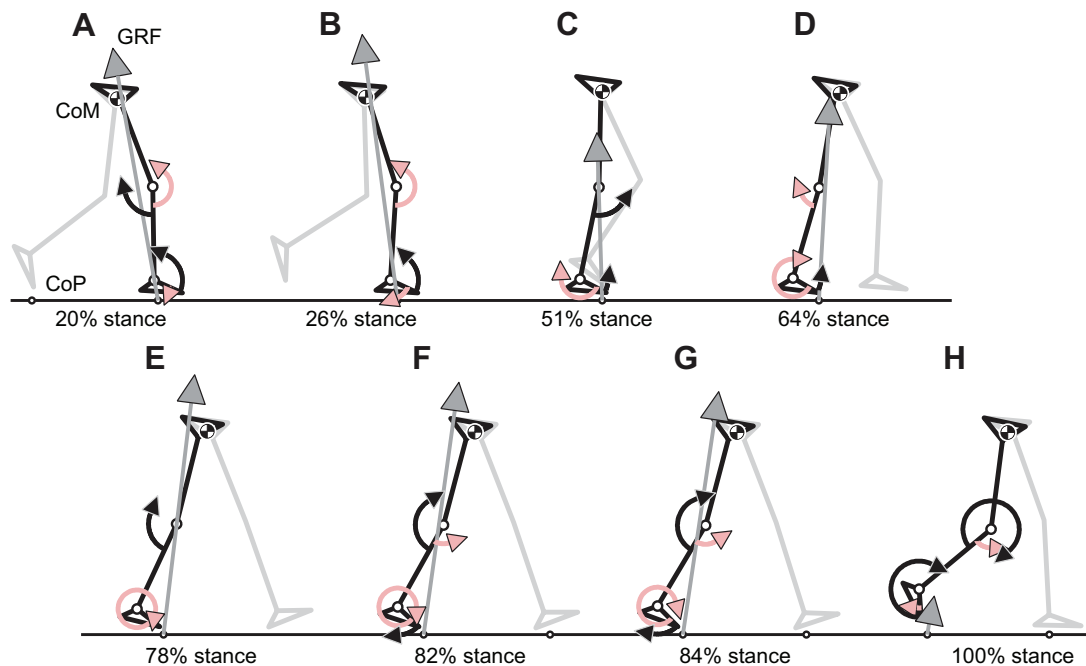


**Fig. 1. Dynamics of the lower limb and ground reaction force (GRF) for the stance phase of one representative subject walking at 75% PTS (preferred transition speed between walking and running;  $1.5 \text{ m s}^{-1}$ ).** Knee and ankle joint torques are displayed as pink arrows around the shank and foot segments, respectively. Black arrows show the amount of angular velocity around the joints. Gray arrows show the GRF. CoM, center of mass; CoP, center of pressure. (A) The foot is flat on the ground with the beginning of single support (at 20% of stance). The GRF flexes both the knee and ankle joint, but flexion is resisted by extending torques in both joints ( $\tau_{Kne}>0$  and  $\tau_{Ank}>0$ ,  $\phi_{Kne}=0$  and  $\phi_{Ank}=0$ ). The GRF has approached the knee joint and has moved further in front of the ankle joint. The extending ankle torque ( $\tau_{Ank}>0$ ) increases, which resists the flexing ankle motion ( $\phi_{Ank}>0$ ). (C) Towards midstance, the extending knee torque decreases with the GRF further approaching the knee joint. At the ankle joint, the GRF moves further in front of the ankle joint. At 51% of stance, the knee torque becomes zero ( $\tau_{Kne}=0$ ), yet the knee still extends ( $\phi_{Kne}>0$ ). The flexing motion in the ankle joint is further decelerated by an increasing extending torque ( $\tau_{Ank}>0$ ,  $\phi_{Ank}<0$ ). (D) At 64% of stance, the knee stops extending and starts flexing ( $\tau_{Kne}<0$ ,  $\phi_{Kne}=0$ ). The GRF has moved in front of the knee joint and further in front of the ankle joint. The flexing motion in the ankle joint is now resisted by a large extending torque ( $\tau_{Ank}>0$ ,  $\phi_{Ank}<0$ ). (E) With zero torque and flexing angular velocity, the knee joint buckles at 78% of stance ( $\tau_{Kne}=0$ ,  $\phi_{Kne}<0$ ). At the same time, the ankle joint is just about to start extending ( $\tau_{Ank}>0$ ,  $\phi_{Ank}=0$ ; beginning of the alleviation phase). (F) Shortly after that, at 82% of stance, the leading leg touches down. The flexing motion of the knee joint is kept under control by a small extending torque ( $\tau_{Kne}>0$ ,  $\phi_{Kne}<0$ ). The extending motion of the ankle joint is accompanied by the extending torque ( $\tau_{Ank}>0$ ,  $\phi_{Ank}>0$ ). (G) With a maximum in angular ankle jerk  $\ddot{\phi}_{Ank}$ , the launching phase begins at 84% of stance, with increasing flexing velocity at the knee joint and increasing extending velocity at the ankle joint. (H) At 100% of stance, i.e. when the trailing leg takes off the ground, fast flexing motion at the knee joint and fast extending motion at the ankle joint are observed.

ankle torque  $\tau_{Ank}$  builds up during single support and is only slightly reduced during the alleviation phase (Fig. 2C). During launching, the major part of this stored energy  $\Delta E_{Ank}$  is released (Table 1). Positive ankle power output  $P_{Ank}$  marks the beginning of the alleviation phase and increases constantly. Its peak of  $\sim 150 \text{ W}$  is not reached until well into the launching phase (Fig. 3A). At the same time, a peak of the extending ankle angular acceleration  $\ddot{\phi}_{Ank}$  is observed (Fig. 3B). This acceleration starts from zero. The angular ankle jerk  $\ddot{\phi}_{Ank}$  (Fig. 3B) shows a maximum shortly after touch-down of the leading leg (TDC). Zero joint torque at the knee joint of the trailing leg allows knee buckling also before TDC (Fig. 2B, Fig. 1E). At the beginning of the launching phase, the knee joint flexes and the ankle joint extends (Fig. 1G). These motions accelerate towards the end of stance.

The vertical momentum  $\vec{p}$  of both the trailing leg (TL) and the remaining body (RB) is redirected during the launching phase at all walking speeds (Fig. 4A, Table 1). A positive  $x$ -component of the TL's impulse vector  $\Delta p_x$  indicates forward acceleration of the TL during this phase at all walking speeds. For the RB,  $\Delta p_x$  is negative at all walking speeds, indicating horizontal deceleration of the RB during launching. The TL's relative impulse  $|\Delta \vec{p}|$  appears larger than that of the RB for all walking speeds, and more than seven times larger at the highest walking speed. Fig. 4B shows the vectors of

velocity change  $\Delta \vec{v}$  for TL and RB during the launching phase at  $1.5 \text{ m s}^{-1}$  [75% PTS (preferred transition speed between walking and running)]. Both vectors indicate a vertical redirection of momentum. While forward velocity  $v_x$  increases for the TL, it decreases for the RB.

The impulses  $\Delta \vec{p}$  of the TL and the RB over both phases of the push-off infer that the ankle joint's power output mostly changes the impulse of the TL (Table 1). In both phases, positive horizontal impulses indicate forward acceleration of the TL ( $\Delta p_x > 0$ ), however, during alleviation, forward acceleration is only small or at most half as much as during launching. In the vertical direction, the TL is decelerated very little or not at all during alleviation ( $\Delta p_y = 0$ ). During launching, the TL is accelerated upward, though a little less at high speeds ( $\Delta p_y > 0$ ). The RB is slightly accelerated forward during alleviation ( $\Delta p_x > 0$ ) and clearly decelerated during launching ( $\Delta p_x < 0$ ). Only at high speeds is the RB vertically accelerated downwards, otherwise it is decelerated during alleviation ( $\Delta p_y < 0$ ). During launching, the RB is accelerated upward ( $\Delta p_y > 0$ ).

Observing the linear joint force power at the hip  $P_{x,Trc}$  and  $P_{y,Trc}$  (Fig. 5E,F), positive power accelerates the head–arms–trunk (HAT) segment forward and negative power decelerates the HAT segment vertically during alleviation. During the launching phase, almost no positive power acts on the HAT segment in either degree of

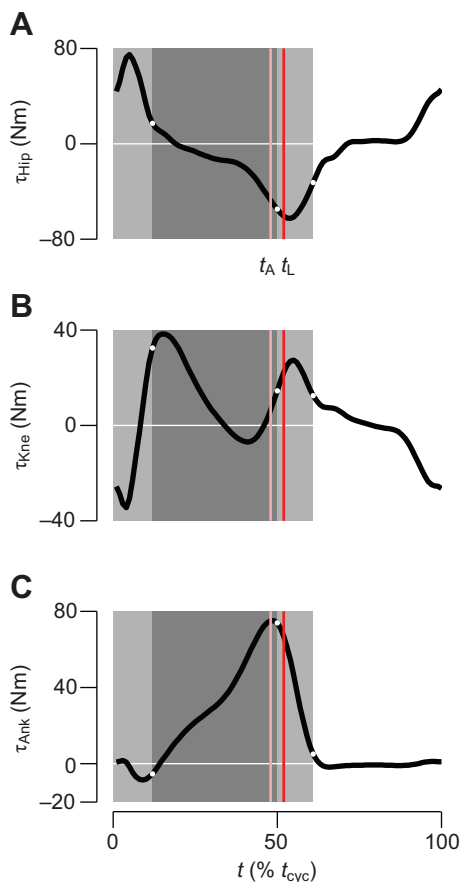


**Fig. 2. Leg joint torques.** Joint torques for the hip ( $\tau_{\text{Hip}}$ ; A), knee ( $\tau_{\text{Knee}}$ ; B) and ankle ( $\tau_{\text{Ank}}$ ; C) for walking at 75% PTS ( $1.5 \text{ m s}^{-1}$ ) of one representative subject. Dark gray areas indicate the single support phase, light gray areas indicate double support phases, and non-shaded areas indicate the swing phase. Vertical lines represent the beginning of the alleviation phase  $t_A$  (beginning of positive ankle power output, where the trailing leg is alleviated from supporting the body mass; pink) and the beginning of the launching phase  $t_L$  (instant of maximum jerk in ankle angle, where stored energy in the ankle joint is released; red). The gait cycle  $t$  is normalized to cycle time and given in %.

freedom. There must be another energy source, possibly from the leading leg, for vertical translation of the HAT segment as  $|\Delta E_{y, \text{Trc}}| > |\Delta E_{\text{Ank}}|$  (Table 1). Transferred power (Fig. 6) during launching is negligible, confirming the observed impulses.

## DISCUSSION

This work is motivated by the controversy about the role of the ankle extensors during late stance in human walking. Do they restore energy lost in collision or do they provide kinetic energy for swing initiation? Literature is lacking knowledge about the biomechanical process leading to high power output of the ankle extensors toward the end of walking stance. Here, we mechanistically elucidate a catapult without escapement. At the same time, we identify the recipient of push-off power by calculating power transfer between the trailing leg and the upper body and their impulses throughout push-off.

In human walking, the foot is flat on the ground for most of the single support phase while the rotating stance leg carries the entire body weight. The kinetic energy of the moving body is converted into elastic potential energy as the ankle extensors are loaded. It is important to note that the ground acts as a block for the flat foot.

Our experimental data clearly show forward traveling of the center of pressure (CoP) increasing the moment arm for external forces (Fig. 1). Additionally, the GRF increases after midstance. Both of these observations indicate that loading of the ankle joint increases throughout single support, leading to a peak in extending ankle torque (Fig. 2C) just before TDC.

The push-off phase at the end of a walking step is usually defined by positive power output in the ankle joint. In model studies it was proposed that positive push-off power can be generated by an instantaneous change of force (Dean and Kuo, 2009; Zelik et al., 2014). For human walking, it is important to note that the ankle extensor muscle fibers are operating near-isometrically during late stance (Fukunaga et al., 2001; Ishikawa et al., 2005; Lichtwark et al., 2007; Cronin et al., 2013), which means they cannot add significant work to the Achilles tendon or the skeleton. Thus, power comes largely from the elastic tendon in series with the muscle fibers and is not provided by active lengthening and shortening of the muscle fibers themselves.

Power is the rate at which energy is converted ( $P = \Delta E / \Delta t$ ). With the ankle extensor fibers adding nearly no work (energy) to the muscle–tendon complex (MTC) during single stance and push-off in walking, conversion of elastic potential energy into kinetic energy faster than the elastic potential energy has been stored implies an increased power output as compared with input. This observed power amplification with the ankle extensor MTC loaded and released elastically must compulsively be related to an accelerated mass, which is accordingly lower during the faster release than during the slower loading. The scenario starts with a static force balance between gravitational force due to the body mass  $m$  ( $F_G = m \cdot g$ ) and the force produced by the ankle extensors ( $F_{\text{MTC}}$ ). Then, leg alleviation is initiated. Now, because of the reduced gravitational force ( $F_G = m_{\text{leg}} \cdot g$ ) of the smaller leg mass  $m_{\text{leg}}$  (approximately one–sixth of the body mass), the force balance becomes dynamic with a corresponding inertial contribution ( $F = m_{\text{leg}} \cdot a_{\text{leg}}$ ). Thus, the leg is accelerated during release.

A catch for this catapult is provided by the extending knee joint and the ground blocking the heel (Fig. 1). Releasing this catch, i.e. initiating knee flexion, closely coincides with the beginning of ankle extensor MTC recoil at ~40% of the gait cycle [compare fig. 2 in Cronin et al. (Cronin et al., 2013) and Fig. 1D]. After that, the conversion of stored elastic potential energy into kinetic energy of the leg segments is started, which rapidly accelerates the ankle into extension. This shows in a sudden change in acceleration from zero, i.e. a jerk, of the extending ankle joint (Fig. 3).

In view of these conditions, the push-off phase can be divided into (1) an alleviation phase, during which the trailing leg is alleviated from supporting the mass of the remaining body, and (2) a launching phase, where the majority of stored elastic energy in the ankle joint is rapidly released to launch the trailing leg into action.

### Alleviation phase

The alleviation phase begins with positive ankle power output in late single support and ends with the maximum rate of change in ankle angular acceleration (jerk). We found the maximum jerk to be a good indicator of complete alleviation of the trailing leg, as a sudden increase in acceleration must be related to a smaller mass. During the alleviation phase, only 10–20% of the energy stored in the ankle extensors  $\Delta E_{\text{Ank}}$  is released (for typical walking speeds, see Table 1). Then, only a small fraction of this work done at the ankle joint is used for horizontal HAT translation via the hip joint. In addition to that, the ratio of transferred horizontal power through the hip joint to angular power generated by the ankle joint  $P_{x, \text{Trc}} / P_{\text{Ank}}$  decreases

Table 1. Impulses and power integrals

Phase	Quantity	Descriptor	25% PTS	50% PTS	75% PTS	100% PTS	125% PTS	
			0.52 m s <sup>-1</sup>	1.04 m s <sup>-1</sup>	1.55 m s <sup>-1</sup>	2.07 m s <sup>-1</sup>	2.59 m s <sup>-1</sup>	
Alleviation phase	$t_A$ (% $t_{cyc}$ )		54.9±2.3	49.6±2.6	43.2±4.3	34.9±5.5	31.3±2.2	
	$\Delta t$ (s)		0.006±0.030	0.038±0.026	0.076±0.044	0.117±0.050	0.119±0.019	
	$ \Delta\vec{p} $ (Ns)	RB		2.7±1.0	3.8±1.9	7.2±6.1	15.9±10.3	19.9±10.3
		TL		1.6±0.5	2.2±0.9	4.8±2.2	7.6±2.8	10.2±3.4
		CoM		3.0±1.2	5.2±2.2	10.2±7.3	19.8±10.5	23.1±10.2
	$\Delta\rho_x$ (Ns)	RB		0.4±0.6	1.1±0.8	1.9±1.3	1.5±1.2	0.3±2.6
		TL		0.0±0.8	1.6±0.9	4.4±2.1	6.9±3.3	9.1±4.0
		CoM		0.4±0.8	2.6±1.6	6.2±3.1	8.3±3.5	9.4±2.9
	$\Delta\rho_y$ (Ns)	RB		0.3±1.7	2.3±2.2	0.1±8.2	-13.1±12.8	-19.0±10.5
		TL		-0.1±0.4	0.2±0.4	-0.6±1.1	-1.2±0.9	-0.9±1.5
		CoM		0.2±2.0	2.5±2.4	-0.5±9.2	-14.2±13.4	-19.8±10.9
	Launching phase	$t_L$ (% $t_{cyc}$ )		55.3±1.2	52.9±1.0	50.9±0.8	48.4±1.1	47.0±1.4
$\Delta t$ (s)			0.158±0.032	0.115±0.012	0.094±0.009	0.091±0.011	0.077±0.009	
$ \Delta\vec{p} $ (Ns)		RB		7.3±2.6	11.4±3.5	18.9±5.9	21.7±6.5	18.4±5.3
		TL		5.3±1.6	8.6±1.7	11.7±2.3	15.5±3.3	17.1±3.7
		CoM		6.5±2.8	12.7±4.3	21.2±6.4	22.5±7.7	15.4±6.6
$\Delta\rho_x$ (Ns)		RB		-5.8±3.0	-5.6±3.2	-8.0±2.9	-9.3±3.2	-12.3±4.3
		TL		4.3±1.8	7.9±1.6	11.0±2.2	15.3±3.2	17.0±3.7
		CoM		-1.5±3.3	2.3±3.0	3.0±3.0	6.0±3.5	4.7±3.8
$\Delta\rho_y$ (Ns)		RB		1.3±3.2	8.8±3.8	16.8±5.7	19.1±6.7	9.0±10.7
		TL		2.6±1.3	3.1±0.9	3.8±1.1	2.1±1.2	0.4±1.9
		CoM		3.9±4.3	11.9±4.3	20.6±6.5	21.2±7.5	9.4±12.1
$ \vec{p}_1 $ (Ns)		RB		33.5±7.3	66.6±12.2	100.4±19.0	132.6±24.4	165.7±29.5
		TL		7.3±2.2	11.0±2.0	15.8±3.0	18.6±4.0	22.6±5.1
$ \Delta\vec{p} $ (% $ \vec{p}_1 $ )		RB		21.6±5.1	16.9±4.1	18.5±3.6	16.3±4.2	11.0±2.2
		TL		81.7±26.0	79.8±11.2	75.0±11.8	87.3±17.2	79.5±16.2
$\Delta\rho_x$ (% $ \vec{p}_1 $ )		RB		-16.7±6.5	-8.3±4.3	-7.9±2.3	-7.0±1.9	-7.4±2.2
		TL		67.9±26.4	73.9±10.9	70.7±11.8	86.2±17.1	78.8±16.3
$\Delta\rho_y$ (% $ \vec{p}_1 $ )		RB		3.8±10.4	12.9±5.4	16.4±3.7	14.4±4.7	5.6±5.9
		TL		39.2±17.9	28.7±6.6	24.3±5.0	11.3±6.5	1.1±8.5
Alleviation phase		$\Delta E$ (J)	x,Trc	-0.06±0.33	0.76±0.75	2.92±2.13	2.14±2.76	-2.28±6.25
	y,Trc		0.09±0.45	-1.72±1.54	-8.24±5.01	-11.66±5.67	-7.63±6.83	
	Ank		0.01±0.74	1.28±1.58	3.84±3.45	9.67±6.65	15.90±8.56	
Launching phase	$\Delta E$ (J)	x,Trc	-0.28±1.38	-1.32±1.44	-2.52±1.53	-5.73±3.73	-18.03±7.90	
		y,Trc	0.88±1.30	0.49±1.56	-1.43±1.77	-5.06±2.89	-4.02±1.97	
		Ank	5.34±2.45	10.09±3.46	14.03±4.96	18.38±5.92	16.98±7.82	

Two phases of push-off are distinguished. The alleviation phase begins with positive ankle power output at the instant  $t_A$  and ends with the instant of maximum jerk in ankle angle at  $t_L$ . The launching phase follows directly after the alleviation phase and ends with the foot taking off the ground (TO). The duration of the alleviation phase and launching phase are denoted by  $\Delta t_A$  and  $\Delta t_L$ , respectively. Norms of the impulse vectors  $|\Delta\vec{p}|$  for both phases are presented for the trailing leg ( $m_{TL}=11.4\pm 1.8$  kg), the remaining body ( $m_{RB}=59.5\pm 9.8$  kg) and the entire body ( $m_{CoM}=70.9\pm 11.7$  kg). Also presented are the impulse components  $\Delta\rho_x$  and  $\Delta\rho_y$ . All data are given as grand means±s.d. of 21 subjects for the five measured walking speeds. Additionally, for the launching phase, the norms of the impulse vectors and their components of TL and RB are normalized to the norm of the respective momentum vector  $|\vec{p}_1|$  at the beginning of this phase  $t_L$  ( $|\Delta\vec{p}|$ ,  $\Delta\rho_x$  and  $\Delta\rho_y$ ). Power integrals  $\Delta E$  for both phases are given for the rotation of the ankle joint (Ank) and the translation of the hip joint (x,Trc and y,Trc). PTS, preferred transition speed between walking and running.

from 1 early in this phase to almost 0 (Fig. 6A). So there is not much that the ankle joint push-off contributes to forward propulsion of the body in this phase.

It is interesting to note that both legs work together horizontally during the alleviation phase (Fig. 5E). This is in contrast to the strict opposing actions of the two legs predicted by conceptual models such as the inverted pendulum or the spring-mass model. The forward acceleration by the leading leg could result from active leg retraction (see positive hip torque before and after touch-down, Fig. 1A). The heel piled into the ground would be the rotation point for the leg and, with the momentum of leg retraction, would cause forward acceleration at the hip joint.

Vertically, the unloading ankle power transfers as negative power through the hip joint. This indicates that the trailing leg brakes the downward movement of the upper body (HAT segment) during the alleviation phase but does not accelerate the HAT segment into

moving upward (Fig. 5F). Energy used for this vertical hip translation is higher than energy produced at the ankle joint (Table 1). It seems most likely that the leading leg is the source of this additional energy. However, at TDc, there is a brief interruption of decelerating the HAT segment's downward movement, which can result in a short period of the HAT segment falling even faster. This is due to the knee forced into flexion after TDc (Fig. 2B), therefore delaying the build-up of leg force.

To summarize, only a small part of the power generated at the ankle joint during alleviation is transferred through the hip joint, which is mostly used to decelerate the falling HAT segment.

#### Launching phase

The launching phase follows directly after the alleviation phase and ends with the trailing leg taking off the ground. Here, peak ankle power is generated. However, most of the power generated at the

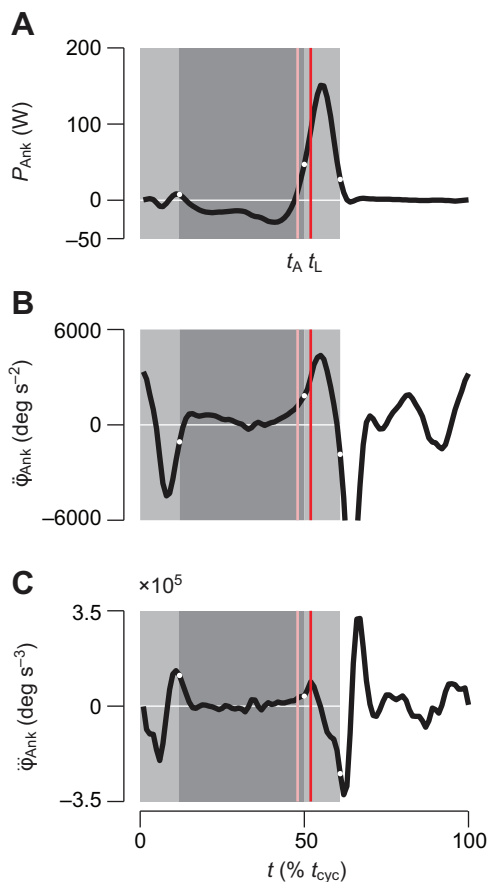


**Fig. 3. Angular joint power, acceleration and jerk at the ankle joint.** Ankle angular joint power  $P_{Ank}$  (A), angular acceleration  $\dot{\varphi}_{Ank}$  (B) and jerk  $\ddot{\varphi}_{Ank}$  (C) for walking at 75% PTS ( $1.5 \text{ m s}^{-1}$ ) of one representative subject. Dark gray areas indicate the single support phase, light gray areas indicate double support phases, and non-shaded areas indicate the swing phase. Vertical lines represent the beginning of the alleviation phase  $t_A$  and the beginning of the launching phase  $t_L$ . The gait cycle is normalized to cycle time and given in %.

ankle joint is not likely to be used for propelling the body forward, as with increasing ankle power there is steady decreasing of the power ratio  $P_{x,Trc}/P_{Ank}$ , which crosses zero even before the ankle power reaches its maximum (see Fig. 3A, Fig. 6A). The power integrals calculated for the launching phase indicate that a major part of the work done at the ankle joint remains within the leg (Table 1). This also shows in the relative impulse  $|\Delta \vec{p}|$ , which is four to eight times higher in the trailing leg than in the remaining body (Table 1).

Our results indicate that the buckling knee joint at the beginning of the launching phase inhibits the transfer of power from the ankle joint to the remaining body. With that, it enables rapid propulsion of the trailing leg into swing (Fig. 4B).

### Collision losses

In accordance with previous findings, our data show rapid unloading of the ankle joint during the launching phase along with a peak in power output (Fig. 2C, Fig. 3A). Work done by the ankle joint has been discussed to cause redirection of the CoM at the step-to-step transition (McGeer, 1990; Donelan et al., 2002a; Donelan et al., 2002b; Kuo, 2002; Collins et al., 2005; Dean and Kuo, 2009; Usherwood et al., 2012; Zelik et al., 2014). It was hypothesized that the trailing leg's push-off along the leg axis reduces the collision loss at touch-down of the leading leg (Kuo, 2002). Also, the

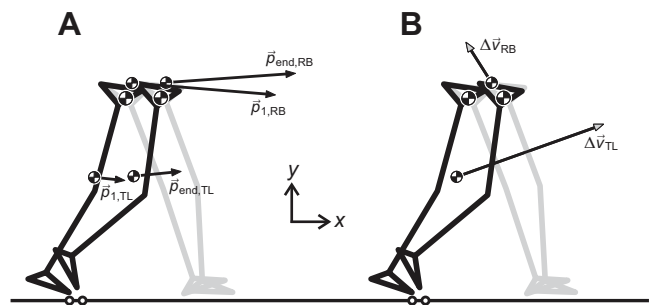


**Fig. 4. Momentum and velocity of the trailing leg and the remaining body during launching.** (A) Momentum of the trailing leg  $\vec{p}_{TL}$  and the remaining body  $\vec{p}_{RB}$  are shown at the beginning and end of the launching phase for walking at 75% PTS ( $1.5 \text{ m s}^{-1}$ ) of one representative subject. The vectors originate in their respective centers of mass (CoM<sub>TL</sub> and CoM<sub>RB</sub>). (B) Change of velocity for the trailing leg  $\Delta \vec{v}_{TL}$  and the remaining body  $\Delta \vec{v}_{RB}$  are plotted at the mid configuration of the launching phase.

appearance of a push-off at or before touch-down was found to be crucial for the reduction of collision losses (Donelan et al., 2002a; Collins et al., 2005). However, our findings indicate that only a small fraction of the energy stored in the ankle joint is transferred along the leg axis with an immediate effect on HAT translation in space. Thus, the push-off in human walking is not primarily there to reduce the collision loss experienced by the HAT, but affects the CoM by its localized action, accelerating the trailing leg. An elastic load transfer from one leg to the other during double support could take care of vertically redirecting and horizontally decelerating the remaining body. In a previous study, it was observed that global elasticity of the human leg can be assumed for the double support phase in walking (Lipfert et al., 2012). This global elastic leg behaviour, regardless of its local mechanical origin, reduces the actual collision losses.

### Conclusions

Our study provides an experimentally supported mechanical scenario for the observed power amplification during push-off in human walking. The push-off phase consists of an alleviation phase and a launching phase. During alleviation, support of the body mass is discontinued by the opposing motions of the knee and ankle joints of the trailing leg (contrasting the in-phase motion of both joints observed in human running). With that, launching is enabled, where the smaller mass of the trailing leg exhibits a powerful acceleration into swing by efficiently utilizing elastic energy storage.

### MATERIALS AND METHODS

#### Data collection

We used experimental data from a previous study (Lipfert, 2010), where three-dimensional (3D) lower limb kinematics and dynamics were collected from 21 subjects (11 females, 10 males) walking at different speeds (25, 50, 75, 100 and 125% of their PTS between walking and running) on an instrumented treadmill (type ADAL-WR, HEF Tecmachine, Andrezieux Boutheon, France). Motion analysis was performed using eight wall-mounted high-speed infrared cameras (Qualisys, Gothenburg, Sweden) recording at a sampling frequency of 240 Hz. For the present study, we used camera recordings of the sagittal positions of eight reflective markers placed over anatomical landmarks of both of the subject's lower limbs (Fig. 7). The center of mass of the HAT segment (CoM<sub>HAT</sub>) was derived from gender-, height- and weight-specific regression curves (NASA, 1978). GRFs were recorded at a frequency of 1000 Hz and were down-sampled to 240 Hz. Kinematic and dynamic data were recorded simultaneously, synchronized by a trigger signal provided by the treadmill computer. The remaining time

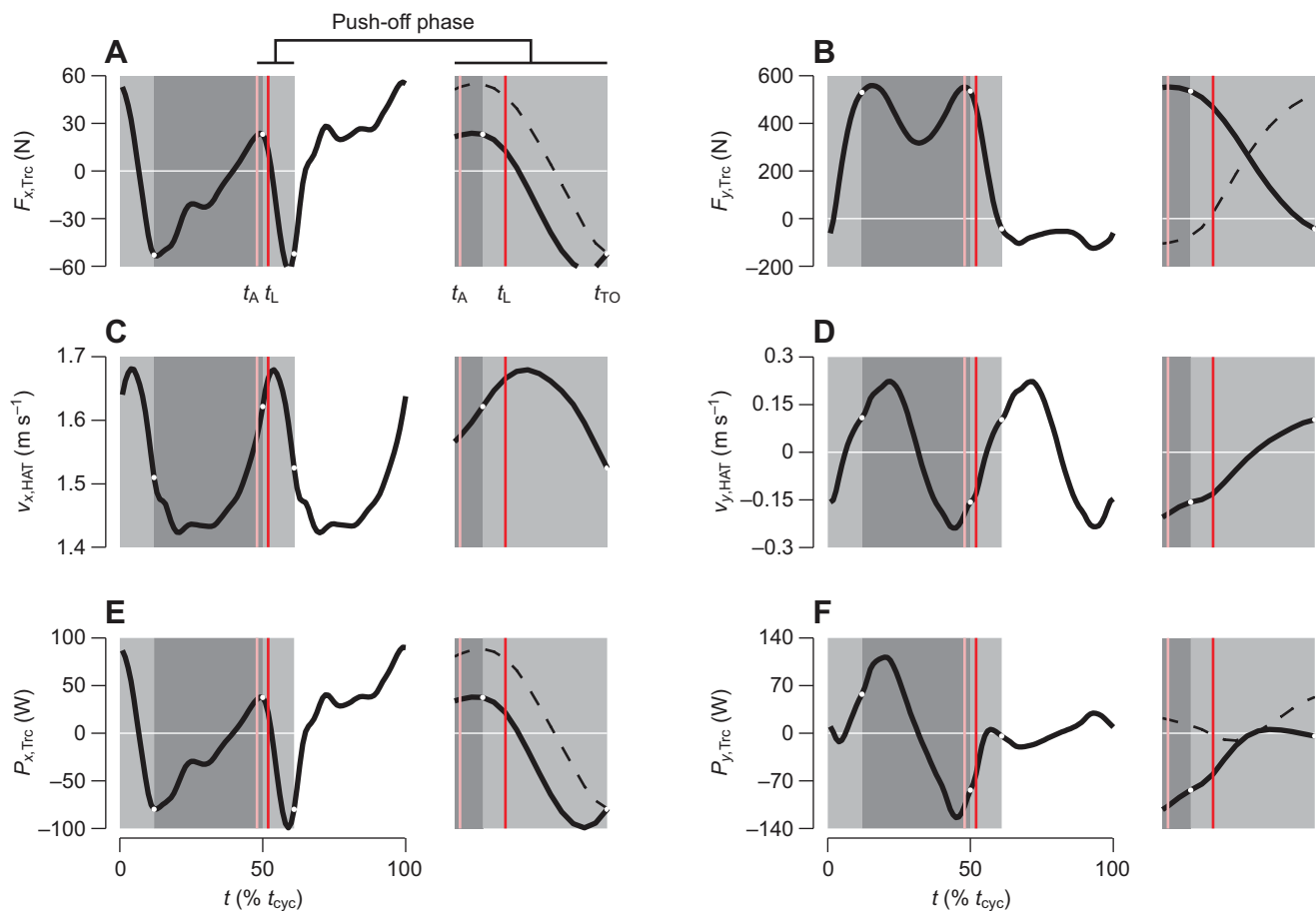


**Fig. 5. Hip joint forces, head–arms–trunk (HAT) segment velocity and linear joint force power at the hip joint.** Hip joint forces  $F_{x,Trc}$  and  $F_{y,Trc}$  (A,B), CoM velocities of the HAT segment  $V_{x,HAT}$  and  $V_{y,HAT}$  (C,D), and the resultant linear hip joint force power  $P_{x,Trc}$  and  $P_{y,Trc}$  (E,F) are presented for walking at 75% PTS ( $1.5 \text{ m s}^{-1}$ ) of one representative subject. Dark gray areas indicate the single support phase, light gray areas indicate double support phases, and non-shaded areas indicate the swing phase. Vertical lines represent the beginning of the alleviation phase  $t_A$  and the beginning of the launching phase  $t_L$ . The gait cycle is normalized to cycle time and given in %. Shown on the right of each double-panel is the horizontal zoom in on the push-off phase. Curves of the leading leg are added as dashed lines. Take-off of the trailing leg is marked by  $t_{TO}$ .

delay ( $2.5 \times 10^{-3} \text{ s}$ ) and time drift ( $2.0 \times 10^{-5} \text{ s s}^{-1}$ ) between both systems were identified and corrected after the measurements (Lipfert et al., 2009).

#### Data processing

All data were processed and analyzed using custom software (MATLAB R2007b, The MathWorks, Inc., Natick, MA, USA). Signals of detected gait cycles (starting at touch-down of one leg and ending with the next touch-down of the same leg) were linearly interpolated to 100 points and then averaged for each subject to give individual means (left and right side combined). In total, we analyzed 5188 walking gait cycles (between 21 and 72 per speed and subject).

CoM movements were determined by twice integrating the accelerations received from GRF data (for details, see Lipfert, 2010).

Definitions of sagittal plane kinematics are illustrated in Fig. 7. The collected marker trajectories were used to define foot, shank, thigh and HAT segments. Absolute segment angles were measured clockwise with respect to the negative  $x$ -axis. Joint angles at the hip ( $\phi_{Hip}$ ), knee ( $\phi_{Knee}$ ) and ankle ( $\phi_{Ank}$ ) were measured between the corresponding two adjacent segments and were defined to increase with joint extension. Angular velocity  $\dot{\phi}$ , acceleration  $\ddot{\phi}$  and jerk  $\dddot{\phi}$  were derived using a central difference approximation. All kinematic data were low-pass filtered using a zero-lag second-order Butterworth filter with a cut-off frequency of 40 Hz (Winter, 2004).

Leg joint torques and forces can be calculated implementing inverse dynamics algorithms. Inconsistencies between inverse dynamics model assumptions (e.g. rigid segments) and measured kinematics (e.g. fluctuating

segment lengths due to skin marker movement) can be identified and corrected. In our analysis, raw skin marker trajectories were processed such that constant segment lengths throughout measured sequences were guaranteed before calculating inverse dynamics. Essentially, we determined sagittal ankle, knee and hip joint torques for each leg by a sequential algorithm based on the sagittal coordinates of four markers per leg (see Appendix 2 for further details). Equations of motion were solved for the sagittal plane taking soft tissue dynamics into account (Günther et al., 2003). We also calculated linear joint force power by multiplying the joint force with the velocity of the adjoining segment's CoM. For details on force, torque and power contributions in a linked chain of segments, see Appendix 2.

After the inverse dynamics procedure, the resulting joint torques  $\tau$  and joint forces  $F_x$  and  $F_y$ , as well as the resultant linear joint force power contributions  $P_x$  and  $P_y$ , were further low-pass filtered with a cut-off frequency of 15 Hz. We defined extending joint torques to be positive, and flexing joint torques to be negative. Ankle joint power  $P_{Ank}$  was calculated by multiplying ankle torque  $\tau_{Ank}$  by ankle angular velocity  $\dot{\phi}_{Ank}$ .

We divided the push-off phase into two functional phases. The alleviation phase begins with positive ankle power output and ends with the instant of maximum jerk in ankle angle. The launching phase begins with the instant of maximum jerk in ankle angle and ends with the foot taking off the ground (Fig. 3).

We noticed automatic detection failing to reliably return corresponding timing of the maximum ankle jerk for individual gait cycles. Because of technical limitations (spatial resolution in particular), the repeated derivation

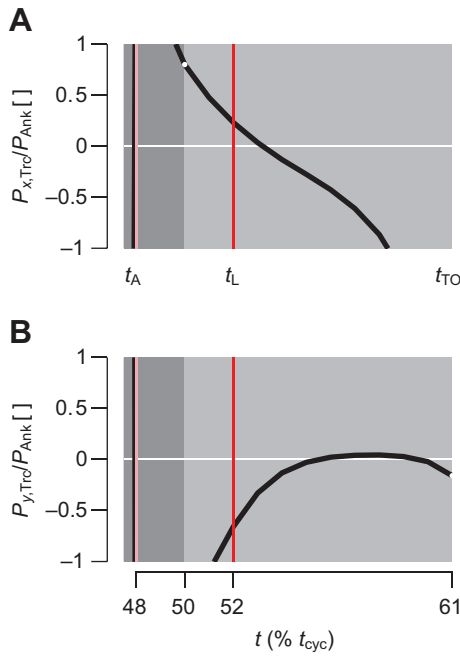


**Fig. 6. Power ratio.** The ratio of linear hip joint force power [horizontal contribution  $P_{x,Trc}$  (A), vertical contribution  $P_{y,Trc}$  (B)] and angular ankle joint power  $P_{Ank}$  is presented for both phases of push-off during walking at 75% PTS ( $1.5 \text{ m s}^{-1}$ ) of one representative subject. As further detailed in Appendix 2,  $P_{Ank}=P_{t,12}$  (indices 1 and 2 for the foot and shank segments, respectively) and  $P_{F,lin,34}=P_{x,Trc}+P_{y,Trc}$ , where  $P_{x,Trc}=F_{x,34} \cdot V_{x,4}$  and  $P_{y,Trc}=F_{y,34} \cdot V_{y,4}$  (indices 3 and 4 for the thigh and HAT segments, respectively). Note the terms  $P_{x,Trc}/P_{Ank}$  and  $P_{y,Trc}/P_{Ank}$  are equivalent to  $dE_{x,Trc}/dE_{Ank}$  and  $dE_{y,Trc}/dE_{Ank}$ , respectively. The dark gray area indicates the last part of single support from  $t_s$  to TDC (touch-down of the leading leg), and the light gray area indicates the double support phase (TDC to TO). Vertical lines represent the beginning of the alleviation phase  $t_A$  and the beginning of the launching phase  $t_L$ . Time is normalized to cycle time and given in %.

of kinematic data collected at only 240 Hz had led to rather ragged time series, which did not always allow clear identification of the right index. Therefore, we opted to manually check each of the analyzed 5188 gait cycles to correct misdetection where necessary. Specifically, we smoothed the jerk further by eye where filtering was useless due to extreme raggedness, which occurred predominantly at the slowest walking speed.

In our study, the angular push-off power generated at the ankle joint can be transferred through the hip joint in three degrees of freedom, two linear and one angular. As angular power transfer through the hip joint does not contribute to propulsion and support of the body, we only considered linear power transfer. For both phases, work  $\Delta E$  was calculated for the hip joint (linear joint work  $\Delta E_{x,Trc}$  and  $\Delta E_{y,Trc}$ , Eqns 1 and 2) and the ankle joint (angular joint work  $\Delta E_{Ank}$ , Eqn 3) by integrating power over time:

$$\Delta E_{x,Trc} = \int_{t_1}^{t_2} P_{x,Trc} dt, \quad (1)$$

$$\Delta E_{y,Trc} = \int_{t_1}^{t_2} P_{y,Trc} dt, \quad (2)$$

$$\Delta E_{Ank} = \int_{t_1}^{t_2} P_{Ank} dt, \quad (3)$$

where  $t_1$  and  $t_2$  specify the beginning and end of each phase, respectively. As further detailed in Appendix 2,  $P_{Ank}=P_{t,12}$  (indices 1 and 2 for the foot and shank segments, respectively) and  $P_{F,lin,34}=P_{x,Trc}$ , where  $P_{x,Trc}=F_{x,34} \cdot V_{x,4}$  and  $P_{y,Trc}=F_{y,34} \cdot V_{y,4}$  (indices 3 and 4 for the thigh and HAT segments, respectively).

We defined the trailing leg (TL) as consisting of three bony segments (foot, shank and thigh) and two wobbling masses (shank and thigh) (Günther et al., 2003), and the remaining body (RB) as the entire body without the

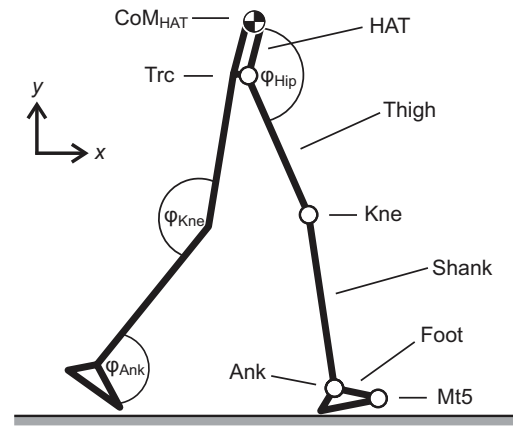


**Fig. 7. Kinematic setup.** Sagittal marker positions are recorded at the hip (greater trochanter, Trc), the knee (lateral knee joint gap, Kne), the toe (fifth metatarsal joint, Mt5), and the ankle (lateral malleolus, Ank). The center of mass (CoM) of the HAT segment is derived from gender-, height- and weight-specific regression curves (NASA, 1978). The foot segment is defined between Mt5 and Ank, the shank segment between Ank and Kne, the thigh segment between Kne and Trc, and the HAT segment between Trc and  $CoM_{HAT}$ . Ankle angle  $\phi_{Ank}$ , knee angle  $\phi_{Kne}$  and hip angle  $\phi_{Hip}$  are defined as inner joint angles between two adjacent segments and increase with joint extension.

TL. The position and momentum of the trailing leg's center of mass  $CoM_{TL}$  were calculated using:

$$x_{CoM,TL} = \frac{\sum_{i=1}^5 m_i \cdot x_i}{m_{TL}}, \quad (4)$$

$$y_{CoM,TL} = \frac{\sum_{i=1}^5 m_i \cdot y_i}{m_{TL}}, \quad (5)$$

$$\vec{p}_{TL} = \sum_{i=1}^5 m_i \begin{pmatrix} v_{x_i} \\ v_{y_i} \end{pmatrix}, \quad (6)$$

where bony segments and wobbling masses are enumerated from 1 to 5. The trailing leg's mass was determined by:

$$m_{TL} = \sum_{i=1}^5 m_i. \quad (7)$$

The position and momentum of the remaining body's center of mass  $CoM_{RB}$  were calculated by Eqns 8–10. The mass of the entire body is denoted by  $m_{CoM}$  and the center of mass position of the entire body by  $x_{CoM}$  and  $y_{CoM}$ .

$$x_{CoM,RB} = \frac{m_{CoM} \cdot x_{CoM} - m_{TL} \cdot x_{CoM,TL}}{m_{CoM} - m_{TL}}, \quad (8)$$

$$y_{CoM,RB} = \frac{m_{CoM} \cdot y_{CoM} - m_{TL} \cdot y_{CoM,TL}}{m_{CoM} - m_{TL}}, \quad (9)$$

$$\vec{p}_{RB} = \begin{pmatrix} m_{CoM} \cdot v_{x,CoM} - p_{x,TL} \\ m_{CoM} \cdot v_{y,CoM} - p_{y,TL} \end{pmatrix}. \quad (10)$$

For both the alleviation and the launching phase, impulses  $\Delta \vec{p}$  were calculated for the TL and RB by subtracting the momentum at the beginning of the phase  $\vec{p}_1$  from the momentum at the end of the phase  $\vec{p}_{end}$ :

$$\Delta \vec{p} = \vec{p}_{end} - \vec{p}_1. \quad (11)$$

For the launching phase, the norm  $|\Delta \vec{p}|$  of  $\Delta \vec{p}$ , as well as the  $x$ - and  $y$ -components, were additionally normalized to the norm of the respective



momentum vector  $|\vec{p}_1|$  at the beginning of the launching phase (maximum jerk in ankle angle).

## APPENDIX 1

### Maximum power output and shortening velocities of the muscle fibers of the soleus and gastrocnemius

The description of force–velocity properties of intact human skeletal muscle and with it the determination of their maximum power capability is not trivial, as muscle forces can not be measured *in vivo* and shortening velocities of contractile elements can only be obtained in experiments under extremely restricted conditions (Herzog, 2007). However, force–velocity relationships may be estimated from muscle parameters and by solving Hill's equation (Hill, 1938).

Muscle parameters for the human soleus (SOL) and gastrocnemius (GAS) muscles available from the literature are summarized in Table A1. Percentages of fiber types were taken from Yamaguchi et al. (Yamaguchi et al., 1990) and were used to weigh parameter values when combining information on slow- and fast-twitch fibers. Maximum active isometric force  $F_{\text{iso}}$  and optimum muscle fiber length  $l_{\text{opt}}$  were averaged from Maganaris (Maganaris, 2001; Maganaris, 2003) and Yamaguchi et al. (Yamaguchi et al., 1990). Maximum shortening velocity  $v_{\text{max}}$  of  $6\text{--}16l_{\text{opt}}\text{ s}^{-1}$  (depending on fiber type) and a curvature of the force–velocity relationship  $C$  of 0.25 are generally assumed to be good average values for skeletal muscle of vertebrates (Alexander, 2006; Herzog, 2007). For  $v_{\text{max}}$  we also took data reported by Bottinelli and others (Bottinelli et al., 1996) and thermal dependence (Bennett, 1984) into account.

The force–velocity relationship  $F(v)$  was calculated for concentric contractions by solving:

$$F(v) = F_{\text{iso}} \cdot \frac{v_{\text{max}} - v}{v_{\text{max}} + v \cdot \frac{1}{C}} \quad (\text{A1})$$

Instantaneous power  $P(v)$  was determined by:

$$P(v) = F(v) \cdot v \quad (\text{A2})$$

Maximum power output  $P_{\text{max}}$  and the corresponding shortening velocity  $v_{P,\text{max}}$  may be read off the power–velocity curve (Fig. A1) or may simply be calculated by solving:

$$P_{\text{max}} = p \cdot F_{\text{iso}} \cdot v_{\text{max}} \quad (\text{A3})$$

and:

$$v_{P,\text{max}} = q \cdot v_{\text{max}} \quad (\text{A4})$$

where  $p$  and  $q$  are factors (here 0.095 and 0.31) depending on  $C$ . Detailed deduction of Eqns A3 and A4 can be traced in Herzog (Herzog, 2007).

Results for the muscles'  $P_{\text{max}}$  and corresponding  $v_{P,\text{max}}$  were 67 W at  $0.06\text{ m s}^{-1}$  ( $1.5l_{\text{opt}}\text{ s}^{-1}$ ) for the SOL and 50 W at  $0.12\text{ m s}^{-1}$  ( $2.4l_{\text{opt}}\text{ s}^{-1}$ ) for the GAS. With that, a maximum total power output of 117 W is given for the ankle extending muscle mass.

**Table A1. Muscle parameters for the human soleus and gastrocnemius muscles**

	$F_{\text{iso}}$ (N)	$v_{\text{max}}$ ( $l_{\text{opt}}\text{ s}^{-1}$ )	$l_{\text{opt}}$ (m)	$C$
Soleus	3500	5.0	0.04	0.25
Gastrocnemius	1300	8.0	0.05	0.25

$F_{\text{iso}}$ , Maximum active isometric force;  $v_{\text{max}}$ , maximum shortening velocity;  $l_{\text{opt}}$ , optimum muscle fiber length;  $C$ , curvature of the force–velocity relationship.

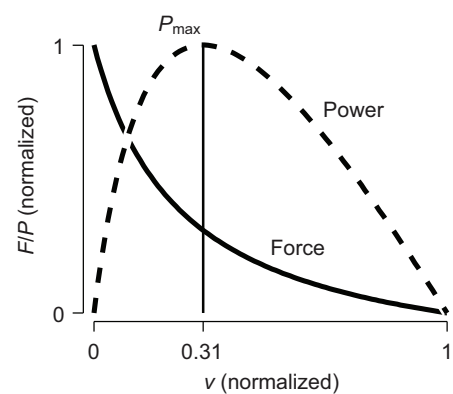


**Fig. A1. Normalized force–velocity and power–velocity relationships for vertebrate skeletal muscle fibers.** Maximum power output  $P_{\text{max}}$  and the corresponding shortening velocity  $v_{P,\text{max}}$  are indicated by the vertical line.

### Maximum power output of the human ankle joint and shortening velocities of the MTUs of the SOL and GAS during walking

When humans walk at a comfortable speed ( $1.3\text{ m s}^{-1}$ ), maximum power output of the extending ankle joint during push-off  $P_{\text{max,Ank}}$  is  $\sim 180\text{ W}$  (Donelan et al., 2002b; Lewis and Ferris, 2008; Silverman et al., 2008; Lipfert, 2010). Thus, higher power output than the muscle fibers of the ankle extensors are capable of seems to be needed for this observed ankle extension. We derived shortening velocities of the MTU for all five walking speeds for the SOL and GAS. MTU length was estimated from our kinematic data (Lipfert, 2010) with moment arms taken from van Soest and Bobbert (van Soest and Bobbert, 1993). The derivative was then calculated to obtain the MTU's shortening velocity  $v_{\text{MTU}}$  (Table A2).

For typical walking speeds, the highest shortening velocities lie above or close to the muscle fibers'  $v_{\text{max}}$ , which would entail no or very little power output  $P_{v,\text{MTU}}$  if it were only muscle mass doing work. For slow walking speeds, the observed maximum power output of the ankle push-off  $P_{\text{max,Ank}}$  may be realized solely by muscle mass; however, the shortening velocity is still approximately as high as 50% of  $v_{\text{max}}$ . If muscle fibers were shortening at these velocities, increased metabolic cost would be the consequence (Alexander, 2006), which is not likely to be happening during a comfortable motion such as very slow walking. Recently published data (Cronin et al., 2013) of one subject walking at  $1.3\text{ m s}^{-1}$  also confirm that muscle fibers of the ankle extensors shorten much slower than the whole MTU, and thus that the muscle fibers do not shorten anywhere near their maximum shortening velocity or provide all of the ankle power.

## APPENDIX 2

### Force, torque and power contributions in a linked chain of segments

A joint is a link or a constraint between two segments or bodies. Here, a segment is represented by one index and a joint by two indices (Fig. A2). The symbol  $P_{F,ij}$  means the power that is transferred from segment  $i$  to segment  $j$  due to the (resultant) 'joint force'  $\vec{F}_{ij}$  that is exerted by segment  $i$  on segment  $j$ . This 'joint force' equals the 'constraint force' in a technical joint only if no force-carrying structures causing a joint torque  $\vec{\tau}_{ij}$  are specified (for  $\vec{\tau}_{ij}$  definition and corresponding equation of motion, see below). In that case,  $\vec{\tau}_{ij}$  is assumed to be caused by two abstract torque generators, one acting on segment  $i$  and one acting on segment  $j$ , respectively. Then, 'joint force' and 'constraint force' would be equivalent terms.

**Table A2. Maximum power output and shortening velocities**

	$P_{max}$ (W)	$v_{P,max}$ (m s <sup>-1</sup> )	$v_{max}$ (m s <sup>-1</sup> )	$v_{MTU}$ (m s <sup>-1</sup> )	$P_{v,MTU}$ (W)	$P_{max,Ank}$ (W)	Walking speed (m s <sup>-1</sup> )
Soleus	67	0.06	0.2	0.11	55	56	0.52
				0.19	7	124	1.04
				0.26	—	206	1.55
				0.32	—	283	2.07
				0.33	—	295	2.59
Gastrocnemius	50	0.12	0.4	0.22	41	56	0.52
				0.34	15	124	1.04
				0.45	—	206	1.55
				0.52	—	283	2.07
				0.53	—	295	2.59
				—	—	—	—

Maximum power output and corresponding shortening velocities of muscle fibers and muscle–tendon units (MTUs) of the ankle extensors as well as maximum power output observed from dynamic data for the ankle joint during five different walking speeds. Note: No power output is given for the MTU at shortening velocities higher than  $v_{max}$ .  $P_{max}$ , maximum power output of muscle fibers;  $v_{P,max}$ , shortening velocity of muscle fibers at their maximum power output;  $v_{max}$ , maximum shortening velocity of muscle fibers;  $v_{MTU}$ , shortening velocity of the MTU observed from kinematic data;  $P_{v,MTU}$ , power output corresponding to  $v_{MTU}$  with regard to the power–velocity relationship (see Fig. A1);  $P_{max,Ank}$ , maximum power output of the extending ankle joint observed from dynamic data.

In the literature, ‘joint forces’ have been analyzed (Quanbury et al., 1975; Robertson and Winter, 1980; Meinders et al., 1998) and ‘resultant joint forces’ have been described (Nigg et al., 2007). Both terms are used in an equivalent sense, so we also denominate  $\vec{F}_{ij}$  simply as ‘joint force’ in the following.

The ‘joint force power’  $P_{F,ij}$  consists of two terms:

$$P_{F,ij} = P_{F,lin,ij} + P_{F,ang,ij} . \tag{A5}$$

The first addend:

$$P_{F,lin,ij} = \vec{F}_{ij} \cdot \vec{V}_j , \tag{A6}$$

is a purely linear term, and the second addend:

$$P_{F,ang,ij} = (\vec{L}_{ji} \times \vec{F}_{ij}) \cdot \vec{\omega}_j , \tag{A7}$$

is a purely angular term, the latter due to the torque that  $\vec{F}_{ij}$  exerts on segment  $j$  (see Eqn A11). Here,  $\vec{V}_j$  is the centre of mass (CoM) velocity of segment  $j$ ,  $\vec{L}_{ji} = \vec{r}_{ji} - \vec{R}_j$  is the vector from the segment’s CoM position  $\vec{R}_j$  to the position  $\vec{r}_{ji} = \vec{r}_{ij}$  of joint  $ij$ ,  $\vec{\omega}_j$  is the angular velocity of segment  $j$ , and ‘ $\cdot$ ’ and ‘ $\times$ ’ are the scalar and the vector product symbols, respectively. We may call the first term in Eqn A5 the ‘linear joint force power’  $P_{F,lin,ij}$  (Eqn A6). The second term in Eqn A5, i.e. the ‘angular joint force power’  $P_{F,ang,ij}$  (Eqn A7), can be

rearranged by circularly shifting the constituents of the scalar triple product, which reformulates Eqn A5 to:

$$\begin{aligned} P_{F,ij} &= \vec{F}_{ij} \cdot \vec{V}_j + (\vec{\omega}_j \times \vec{L}_{ji}) \cdot \vec{F}_{ij} \\ &= \vec{F}_{ij} \cdot (\vec{V}_j + \vec{\omega}_j \times \vec{L}_{ji}) \\ &= \vec{F}_{ij} \cdot \vec{v}_{ij} , \end{aligned} \tag{A8}$$

where  $\vec{v}_{ij} = \vec{V}_j + \vec{\omega}_j \times \vec{L}_{ji}$  symbolizes the velocity of the joint position at which segment  $i$  exerts the joint force  $\vec{F}_{ij}$  on segment  $j$ . Vice versa, due to *actio=reactio*, the reaction force  $\vec{F}_{ji} = -\vec{F}_{ij}$  is exerted by segment  $j$  back on segment  $i$ .

By definition, the joint torque  $\vec{\tau}_{ij}$  represents all torque contributions by structures spanning the joint  $ij$  that are not due to the joint force  $\vec{F}_{ij}$ . The joint torque  $\vec{\tau}_{ij}$  is defined as an internal torque constituting a cause of the angular acceleration of segment  $j$ , which independently superposes the torque due to the joint force  $\vec{F}_{ij}$  (see Eqn A11). ‘Internal’ means that such constituents do not change the overall angular momentum of the mass distribution of the segmented chain connected by all the joints  $ij$ . That is, by such definition,  $\vec{\tau}_{ji} = -\vec{\tau}_{ij}$  pertains in a (force-analogous) torque rule to *actio=reactio*. Like the joint torque  $\vec{\tau}_{ij}$  and the joint force  $\vec{F}_{ij}$  are independent variables in the equations of motion (Eqns A10, A11), the ‘joint torque power’:

$$P_{\tau,ij} = \vec{\tau}_{ij} \cdot \vec{\omega}_j , \tag{A9}$$

is transmitted from segment  $i$  to segment  $j$  independently from the joint force power  $P_{F,ij}$ . In contrast to  $P_{F,ij}$ , consisting of the sum of distinctly linear and angular power contributions, the contribution  $P_{\tau,ij}$  solely changes the angular energy of segment  $j$ .

**Equations of motion**

Eqns A5–A9 are derived from the equations of motion of the free rigid body that represents the segment  $j$  connected by a distal joint  $jj-1$  to its distal neighbor  $j-1$  and a proximal joint  $jj+1$  to its proximal neighbor  $j+1$  within a chain of segments. The segment’s mass  $m_j$  is a scalar parameter. The moment of inertia  $\underline{\theta}_j$  for rotating around the segment’s CoM is a tensor of second order in case of three-dimensional rotations, which is then determined by three principal components, while it is a scalar parameter in a two-dimensional movement description as in this study. In the following, the dot ‘ $\cdot$ ’ means the first time derivative; accordingly, a double dot ‘ $\ddot{\phantom{x}}$ ’ means the second derivative.

The equations of motion of segment  $j$  consist of a linear equation (in general, three components in three-dimensional space, but only

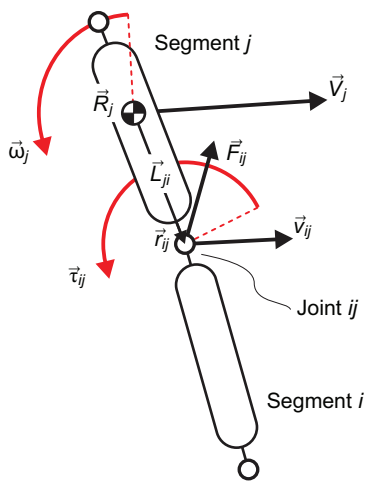


**Fig. A2. Example of a linked chain of segments.** Vectors are joint force  $\vec{F}_{ij}$ , joint torque  $\vec{\tau}_{ij}$ , CoM position  $\vec{R}_j$  of segment  $j$ , position  $\vec{r}_{ij}$  of joint  $ij$ , vector  $\vec{L}_{ji}$  from  $\vec{R}_j$  to  $\vec{r}_{ij}$ , CoM velocity  $\vec{V}_j$  of segment  $j$ , velocity  $\vec{v}_{ij}$  of joint  $ij$ , and angular velocity  $\vec{\omega}_j$  of segment  $j$  around its CoM.

two components in this study) for the segment's CoM position  $\vec{R}_j$  (measured with respect to the inertial system):

$$m_j \cdot \ddot{\vec{R}}_j = \vec{F}_{j-1j} + \vec{F}_{j+1j} + \sum_k \vec{F}_{\text{ext},kj}, \quad (\text{A10})$$

where  $\sum_k \vec{F}_{\text{ext},kj}$  symbolizes the sum over all other (external; index  $k$ ) forces acting on segment  $j$  in addition to the joint forces  $\vec{F}_{j-1j}$  and  $\vec{F}_{j+1j}$ , and an angular equation (also generally three components; only one component in this study) for the segment's angular orientation  $\vec{\phi}_j$  in the inertial system:

$$\underline{\underline{\theta}}_j \cdot \ddot{\vec{\phi}}_j = \vec{L}_{jj-1} \times \vec{F}_{j-1j} + \vec{L}_{jj+1} \times \vec{F}_{j+1j} + \vec{\tau}_{j-1j} + \vec{\tau}_{j+1j} + \sum_m \vec{\tau}_{\text{ext},mj}, \quad (\text{A11})$$

where  $\sum_m \vec{\tau}_{\text{ext},mj}$  symbolizes the sum over all other (external; index  $m$ ) torques acting on segment  $j$  in addition to the torques by the joint forces  $\vec{L}_{jj-1} \times \vec{F}_{j-1j}$  and  $\vec{L}_{jj+1} \times \vec{F}_{j+1j}$ , and the joint torques  $\vec{\tau}_{j-1j}$  and  $\vec{\tau}_{j+1j}$ . The symbol  $\ddot{\vec{\phi}}_j = \ddot{\omega}_j$  represents the angular acceleration, and  $\dot{\vec{\phi}}_j = \dot{\omega}_j$  is another notation for the angular velocity, which already occurs in Eqn A7.

### Constant segment lengths

Applying the formalism of rigid body dynamics for inverse dynamics, modeling of human locomotion is based on the assumption that human bones are rigid. Therefore, we slightly modified the marker coordinates defining the shank and thigh segments to increase consistency of the input data set with the rigid body model assumption (Fig. A3). The corresponding solution to this constant segment length problem has been described by Günther et al. (Günther et al., 2003). Allowing for a weighted combination of a number of discriminative solutions at any given sample, we further enhanced the procedure as follows.

A critical prerequisite was to set a nominal value for the constant segment length, which was near its maximum within a measured sequence but neglected high-value outliers. We gained a reliable and robust determination of constant segment length by taking the median across each sequence. As there is basically no phase shift between ankle marker accelerations and the respective ground reaction forces, even in heavier impact situations (Günther et al., 2003), we relied on the measured  $x$ - and  $y$ -components of the ankle marker (Ank). We further relied on two of the four sagittal components from the knee (Kne) and hip (Trc) markers. Now, the remaining two components could be recalculated where constant lengths for the shank and thigh segments were presumed. Five combinations of relying on and recalculating marker components were possible: (1) relying on the  $x$ -components of Kne and Trc, while recalculating both  $y$ -components, (2) relying on the  $y$ -components of Kne and Trc, while recalculating both  $x$ -components, (3) relying on the  $x$ -component of Kne and the  $y$ -component of Trc, while recalculating the  $y$ -component of Kne and the  $x$ -component of Trc, (4) relying on the  $y$ -component of Kne and the  $x$ -component of Trc, while recalculating the  $x$ -component of Kne and the  $y$ -component of Trc, and (5) relying on the  $x$ - and  $y$ -components of Trc, while recalculating the  $x$ - and  $y$ -components of Kne.

At each point in time a linearly weighted combination of these five solutions, momentarily neglecting the required nominal values of both segment lengths, was calculated. This transient solution was then taken as the initial condition for a recalculation at the same instant. Within approximately five steps the so-implemented iteration converged to modified Kne and Trc marker positions with

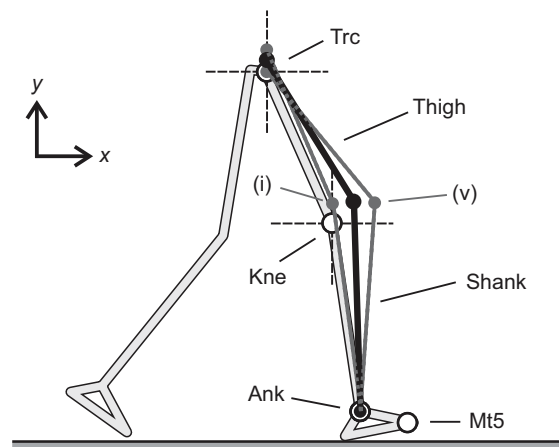


**Fig. A3. Example of marker modification utilizing two constraint combinations.** Sagittal knee (Kne) and hip (Trc) marker coordinates are modified relying on the ankle (Ank) marker position assuming constant lengths of shank and thigh. Original marker data are denoted by the open circles. Modified marker data obtained from constraint combination (i) and (v) are displayed in dark gray. A final solution (black) was obtained after approximately five iterations of recalculating at each point in time.

both segment lengths at their nominal values. The requested relative precision was set to lie between  $10^{-6}$  and  $10^{-8}$ . There were no samples without a final solution. Constant segment lengths and smooth trajectories over time resulted for all measured trials. To demonstrate this procedure, an example of marker modification in reduced form is shown in Fig. A3 for only two constraint combinations (1 and 5). In our analysis, all five equally weighted constraint combinations were included. The exact contribution of each solution at each point in time was not determined.

### Inverse dynamics

The two-dimensional inverse dynamics procedure used here has been detailed by Günther et al. (Günther et al., 2003). Rigid body dynamics determined the equations of motion of the human leg (see Eqns A10, A11) and were sequentially solved for the joint forces and torques at each time sample, starting with the foot-ground interaction. GRF and point of force application were determined from force plate measurements. The corrected marker positions were taken as centers of joint rotation as well as distal and proximal ends of the segments. With that, marker kinematics determined both the application points of joint forces as well as linear and angular kinematics of the segment masses. Segmental anthropometry was derived from gender-, height- and weight-specific regression curves (NASA, 1978) implemented in C code (Hahn, 1993). A point mass coupled with a rigid segment mass by three nonlinear spring-damper elements was used to represent wobbling masses. Their kinematics were calculated from coupling forces known as functions of rigid segment and wobbling mass positions and velocities. The latter are state variables for integrating second-order dynamics of wobbling masses along a time scale, dragged by measured bony segment kinematics, with a simple Runge-Kutta algorithm (Press et al., 1994). Initial conditions of a wobbling mass were assumed to equal those of its corresponding bone CoM. In our study, these three coupling forces incur as external forces in Eqns A10 and A11. The bony segment equations of motion were simultaneously solved for the joint forces and joint torques sample by sample. The coupling parameters of the nonlinear spring-damper elements were taken from Günther et al. (Günther et al., 2003).

**Acknowledgements**

The authors thank Sten Grimmer for his continuous support during the preparation of this paper.

**Competing interests**

The authors declare no competing financial interests.

**Author contributions**

S.L. organized and executed all data collection and data processing except for inverse dynamics procedures. M.G. implemented inverse dynamics procedures and prepared Appendix 2. S.L., M.G. and D.R. contributed to the conception and design of the study, the analyses and the writing of the manuscript. A.S. shared funding and equipment for the study and contributed to the writing of the manuscript.

**Funding**

This study was funded by grant SE 1042/1 to A.S. provided by the Deutsche Forschungsgemeinschaft (DFG).

**References**

- Alexander, R. M. (1988). *Elastic Mechanisms in Animal Movement*. Cambridge: New York, NY: Cambridge University Press.
- Alexander, R. M. (2006). *Principles of Animal Locomotion*. Princeton, NJ: Woodstock: Princeton University Press.
- Alexander, R. M. and Bennet-Clark, H. C. (1977). Storage of elastic strain energy in muscle and other tissues. *Nature* **265**, 114-117.
- Bajd, T., Stefancic, M., Matjacić, Z., Kralj, A., Savrin, R., Benko, H., Karcnik, T. and Obreza, P. (1997). Improvement in step clearance via calf muscle stimulation. *Med. Biol. Eng. Comput.* **35**, 113-116.
- Bennet-Clark, H. C. (1975). The energetics of the jump of the locust *Schistocerca gregaria*. *J. Exp. Biol.* **63**, 53-83.
- Bennett, A. F. (1984). Thermal dependence of muscle function. *Am. J. Physiol.* **247**, R217-R229.
- Blickhan, R. (1989). The spring-mass model for running and hopping. *J. Biomech.* **22**, 1217-1227.
- Bottinelli, R., Canepari, M., Pellegrino, M. A. and Reggiani, C. (1996). Force-velocity properties of human skeletal muscle fibres: myosin heavy chain isoform and temperature dependence. *J. Physiol.* **495**, 573-586.
- Burrows, M. (2003). Biomechanics: frog hopper insects leap to new heights. *Nature* **424**, 509.
- Cavagna, G. A., Saibene, F. P. and Margaria, R. (1964). Mechanical work in running. *J. Appl. Physiol.* **19**, 249-256.
- Collins, S., Ruina, A., Tedrake, R. and Wisse, M. (2005). Efficient bipedal robots based on passive-dynamic walkers. *Science* **307**, 1082-1085.
- Cronin, N. J., Prilutsky, B. I., Lichtwark, G. A. and Maas, H. (2013). Does ankle joint power reflect type of muscle action of soleus and gastrocnemius during walking in cats and humans? *J. Biomech.* **46**, 1383-1386.
- Dean, J. C. and Kuo, A. D. (2009). Elastic coupling of limb joints enables faster bipedal walking. *J. R. Soc. Interface* **6**, 561-573.
- Donelan, J. M., Kram, R. and Kuo, A. D. (2002a). Mechanical work for step-to-step transitions is a major determinant of the metabolic cost of human walking. *J. Exp. Biol.* **205**, 3717-3727.
- Donelan, J. M., Kram, R. and Kuo, A. D. (2002b). Simultaneous positive and negative external mechanical work in human walking. *J. Biomech.* **35**, 117-124.
- Fukunaga, T., Kubo, K., Kawakami, Y., Fukashiro, S., Kanehisa, H. and Maganaris, C. N. (2001). *In vivo* behaviour of human muscle tendon during walking. *Proc. Biol. Sci.* **268**, 229-233.
- Gronenberg, W. (1996). Fast actions in small animals: springs and click mechanisms. *J. Comp. Physiol. A* **178**, 727-734.
- Günther, M., Sholukha, V. A., Kessler, D., Wank, V. and Blickhan, R. (2003). Dealing with skin motion and wobbling masses in inverse dynamics. *J. Mech. Med. Biol.* **3**, 309-335.
- Hahn, U. (1993). *Entwicklung Mehrgliedriger Modelle zur Realistischen Simulation Dynamischer Prozesse in Biologischen Systemen*. Master's thesis, Eberhard-Karls-Universität, Tübingen, Germany.
- Heglund, N. C., Fedak, M. A., Taylor, C. R. and Cavagna, G. A. (1982). Energetics and mechanics of terrestrial locomotion. IV. Total mechanical energy changes as a function of speed and body size in birds and mammals. *J. Exp. Biol.* **97**, 57-66.
- Herzog, W. (2007). Biological materials: muscle. In *Biomechanics of the Musculo-Skeletal System*, 3rd edn (ed. B. Nigg and W. Herzog), pp. 169-217. Hoboken, NJ: John Wiley & Sons Inc.
- Hill, A. V. (1938). The heat of shortening and the dynamic constants of muscle. *Proc. R. Soc. B* **126**, 136-195.
- Hof, A. L. (1998). *In vivo* measurement of the series elasticity release curve of human triceps surae muscle. *J. Biomech.* **31**, 793-800.
- Hof, A. L., Geelen, B. A. and Van den Berg, J. (1983). Calf muscle moment, work and efficiency in level walking: role of series elasticity. *J. Biomech.* **16**, 523-537.
- Hof, A. L., Nauta, J., van der Knaap, E. R., Schallig, M. A. A. and Struwe, D. P. (1992). Calf muscle work and segment energy changes in human treadmill walking. *J. Electromyogr. Kinesiol.* **2**, 203-216.
- Ishikawa, M., Komi, P. V., Grey, M. J., Lepola, V. and Brüggemann, G. P. (2005). Muscle-tendon interaction and elastic energy usage in human walking. *J. Appl. Physiol.* **99**, 603-608.
- Kuo, A. D. (2002). Energetics of actively powered locomotion using the simplest walking model. *J. Biomech. Eng.* **124**, 113-120.
- Lewis, C. L. and Ferris, D. P. (2008). Walking with increased ankle pushoff decreases hip muscle moments. *J. Biomech.* **41**, 2082-2089.
- Lichtwark, G. A. and Wilson, A. M. (2006). Interactions between the human gastrocnemius muscle and the Achilles tendon during incline, level and decline locomotion. *J. Exp. Biol.* **209**, 4379-4388.
- Lichtwark, G. A., Bougoulas, K. and Wilson, A. M. (2007). Muscle fascicle and series elastic element length changes along the length of the human gastrocnemius during walking and running. *J. Biomech.* **40**, 157-164.
- Lipfert, S. W. (2010). *Kinematic and Dynamic Similarities Between Walking and Running*. Hamburg: Verlag Dr Kovac.
- Lipfert, S. W., Günther, M. and Seyfarth, A. (2009). Diverging times in movement analysis. *J. Biomech.* **42**, 786-788.
- Lipfert, S. W., Günther, M., Renjewski, D., Grimmer, S. and Seyfarth, A. (2012). A model-experiment comparison of system dynamics for human walking and running. *J. Theor. Biol.* **292**, 11-17.
- Maganaris, C. N. (2001). Force-length characteristics of *in vivo* human skeletal muscle. *Acta Physiol. Scand.* **172**, 279-285.
- Maganaris, C. N. (2003). Force-length characteristics of the *in vivo* human gastrocnemius muscle. *Clin. Anat.* **16**, 215-223.
- McGeer, T. (1990). Passive dynamic walking. *Int. J. Robot. Res.* **9**, 62-82.
- McMahon, T. A. and Cheng, G. C. (1990). The mechanics of running: how does stiffness couple with speed? *J. Biomech.* **23 Suppl.** **1**, 65-78.
- Meinders, M., Gitter, A. and Czerniecki, J. M. (1998). The role of ankle plantar flexor muscle work during walking. *Scand. J. Rehabil. Med.* **30**, 39-46.
- NASA (1978). *Anthropometric Source Book*, Technical Report 1024, I-III. Hampton, VA: NASA Scientific and Technical Information Office.
- Nigg, B., Stefanyszyn, D. and Denoth, J. (2007). Biological materials: muscle. In *Biomechanics of the Musculo-Skeletal System*, 3 edn (ed. B. Nigg and W. Herzog), pp. 5-18. Hoboken, NJ: John Wiley & Sons Inc.
- Nishikawa, K. C. (1999). Neuromuscular control of prey capture in frogs. *Philos. Trans. R. Soc. B* **354**, 941-954.
- Patek, S. N., Nowroozi, B. N., Baio, J. E., Caldwell, R. L. and Summers, A. P. (2007). Linkage mechanics and power amplification of the mantis shrimp's strike. *J. Exp. Biol.* **210**, 3677-3688.
- Press, W., Teukolsky, S., Vetterling, W. and Flannery, B. (1994). *Numerical Recipes in C – The Art of Scientific Computing*, 2nd edn. Cambridge: Cambridge University Press.
- Quanbury, A., Winter, D. and Reimer, G. (1975). Instantaneous power and power flow in body segments during walking. *J. Hum. Movement Studies* **1**, 59-67.
- Roberts, T. J., Marsh, R. L., Weyand, P. G. and Taylor, C. R. (1997). Muscular force in running turkeys: the economy of minimizing work. *Science* **275**, 1113-1115.
- Robertson, D. G. and Winter, D. A. (1980). Mechanical energy generation, absorption and transfer amongst segments during walking. *J. Biomech.* **13**, 845-854.
- Sawicki, G. S., Lewis, C. L. and Ferris, D. P. (2009). It pays to have a spring in your step. *Exerc. Sport Sci. Rev.* **37**, 130-138.
- Silverman, A. K., Fey, N. P., Portillo, A., Walden, J. G., Bosker, G. and Neptune, R. R. (2008). Compensatory mechanisms in below-knee amputee gait in response to increasing steady-state walking speeds. *Gait Posture* **28**, 602-609.
- Usherwood, J. R., Channon, A. J., Myatt, J. P., Rankin, J. W. and Hubel, T. Y. (2012). The human foot and heel-sole-toe walking strategy: a mechanism enabling an inverted pendular gait with low isometric muscle force? *J. R. Soc. Interface* **9**, 2396-2402.
- van Soest, A. J. and Bobbert, M. F. (1993). The contribution of muscle properties in the control of explosive movements. *Biol. Cybern.* **69**, 195-204.
- Wilson, A. M., Watson, J. C. and Lichtwark, G. A. (2003). Biomechanics: a catapult action for rapid limb protraction. *Nature* **421**, 35-36.
- Winter, D. A. (2004). *Biomechanics and Motor Control of Human Movement*, 3rd edn. New York, NY: John Wiley & Sons, Inc.
- Winter, D. A. and Robertson, D. G. E. (1978). Joint torque and energy patterns in normal gait. *Biol. Cybern.* **29**, 137-142.
- Yamaguchi, G., Sawa, A., Moran, D., Fessler, M. and Winters, J. (1990). A survey of human musculotendon actuator parameters. In *Multiple Muscle Systems: Biomechanics and Movement Organization* (ed. J. Winters and S.-Y. Woo), pp. 717-773. New York, NY: Springer.